InSight's Earth Departure For Mars

Introduction

The Interior Exploration using Seismic Investigations, Geodesy and Heat Transport (InSight) robotic spacecraft began its journey to the surface of Mars on 5 May 2018 at 11:05:00 UTC, the opening of a 2-hour launch window that day. This window was the first in a daily sequence extending to 8 June 2018[1] as dictated by performance from the Atlas V 401 launch vehicle and its Centaur-2 second stage.

Performance was also affected by InSight launch location, Vandenberg Air Force Base (VAFB) Space Launch Complex 3 East (SLC-3E). As a consequence of this choice, InSight is the first interplanetary space mission to be launched from VAFB. With a total InSight launch mass of 694 kg (of which the lander is 358 kg) [1, p. 13], Atlas V 401 performance is adequate to support launch from Cape Canaveral Air Force Station (CCAFS) with even greater margins than at VAFB. So why was a U.S. West Coast launch planned? The decision was based on predictions of more numerous potential schedule conflicts at CCAFS.[2] Launch provider United Launch Alliance (ULA) also benefitted from a more balanced VAFB/CCAFS employee workload in 2018 with InSight being launched from VAFB.

This paper has two objectives. First, assuming launch vehicle performance limits are not in play, it aims to explain how VAFB (or virtually any Earthly location) can target Mars without any plane-altering "dogleg" trajectory deviations following launch. This will be done using VAFB as launch site and some InSight mission parameters as a relevant example of interplanetary trajectory design. A relatively precise reconstruction of InSight's as-flown launch and Earth departure trajectory intercepting Mars are the focus of this paper's second objective. Significant differences between the designed and reconstructed as-flown trajectories will be noted.

Coplanar Trajectory Design Leading To Earth Departure For Mars

In addition to adopting patched conic theory [2, pp. 96-98], this design makes the simplifying assumption a Mars-bound spacecraft undergoes instantaneous VAFB launch into a circular Earth parking orbit whose height above the equator $H = +185$ km. Furthermore, the parking orbit is departed with an instantaneous trans-Mars injection (TMI) impulse whose change-in-velocity vector $\boldsymbol{\Delta v}$ is purely prograde. Though not exact, this trajectory design serves as a reality check when compared with the as-flown InSight reconstruction to follow.

Patched conic design is initiated by generating solutions to the Lambert boundary value problem producing Sun-centered transfer ellipses from Earth to Mars. In addition to the Earth departure

[1] Reference https://mars.nasa.gov/insight/mission/timeline/launch/launch-windows/ (accessed 22 May 2018).
[2] Per the report published 27 March 2018 at http://spacenews.com/efforts-underway-to-ease-floridas-space-coast-launch-congestion/ (accessed 8 May 2018), CCAFS Range Safety has supported at most two launches within 3 days. This constraint may soon evolve to at most two launches in 24 hours, but other Range Safety limitations (at most 48 launches per year, for example) are in play. Also note that, on multiple occasions circa 1966, CCAFS supported two launches (the first being an uncrewed "target"; the second being a crewed Gemini "chaser") within hours of each other to conduct rendezvous/docking flight tests. See https://en.wikipedia.org/wiki/Gemini_8 (accessed 8 May 2018) for an example.

time t_D and Mars arrival time t_A, specified Lambert boundary values target only Type I "short way" trajectories each subtending a heliocentric transfer angle $0 < \theta < 180°$. Earth's heliocentric velocity vector at t_D can be subtracted from heliocentric Earth departure velocity in a transfer ellipse at t_D to define multiple geocentric parameters of relevance to spacecraft trajectory design.

Short way Lambert solutions are summarized in a pork chop chart (PCC), each of whose columns corresponds to a specific t_D and each of whose rows corresponds to a specific t_A. Figure 1's PCC summarizes geocentric asymptotic Earth departure speed v_D, a parameter easily related to launch vehicle performance.[3] Figure 2 summarizes geocentric asymptotic Earth departure declination δ_D. Parking orbit inclination i must obey the constraint $i \geq | \delta_D |$, or the purely prograde TMI assumption is violated. And, as with any launch from a site at latitude ϕ, $i < | \phi |$ doglegs can result in launch vehicle performance losses even greater than those for $i > | \phi |$.

◇	A	B	C	D	E	F	G	H	I	J	K
1	**Mars Arrive**					**Earth Depart Date**					
2	**Date**	4/5/18	4/15/18	4/25/18	5/5/18	5/15/18	5/25/18	6/4/18	6/14/18	6/24/18	7/4/18
3	6/9/18	17.009	19.148	22.539	28.235	38.972	64.731	194.328			
4	6/19/18	13.655	14.900	16.822	19.867	25.007	34.777	58.009	174.599		
5	6/29/18	11.161	11.880	12.997	14.724	17.490	22.258	31.183	52.333	158.069	
6	7/9/18	9.257	9.652	10.297	11.306	12.897	15.555	20.020	28.349	47.959	145.247
7	7/19/18	7.781	7.967	8.325	8.918	9.875	11.497	14.093	18.439	26.463	45.028
8	7/29/18	6.629	6.676	6.854	7.199	7.796	8.867	10.556	13.241	17.662	25.569
9	8/8/18	5.730	5.682	5.744	5.939	6.329	7.098	8.310	10.194	13.106	17.667
10	8/18/18	5.037	4.920	4.907	5.012	5.284	5.886	6.840	8.303	10.474	13.606
11	8/28/18	4.513	4.343	4.281	4.331	4.540	5.051	5.863	7.091	8.857	11.265
12	9/7/18	4.135	3.918	3.820	3.838	4.013	4.477	5.208	6.296	7.820	9.812
13	9/17/18	3.883	3.618	3.489	3.485	3.643	4.082	4.763	5.761	7.126	8.856
14	9/27/18	3.751	3.421	3.260	3.238	3.384	3.807	4.452	5.386	6.639	8.189
15	10/7/18	3.747	3.315	3.112	3.069	3.202	3.609	4.226	5.109	6.277	7.695
16	10/17/18	3.915	3.295	3.028	2.956	3.072	3.461	4.051	4.889	5.990	7.306
17	10/27/18	4.432	3.372	3.000	2.886	2.977	3.344	3.905	4.704	5.747	6.982
18	11/6/18	6.201	3.600	3.026	2.849	2.906	3.245	3.778	4.538	5.531	6.698
19	11/16/18	27.870	4.196	3.117	2.842	2.853	3.160	3.660	4.384	5.331	6.439
20	11/26/18	61.780	6.714	3.320	2.863	2.816	3.083	3.549	4.236	5.141	6.197
21	12/6/18	61.942	60.284	3.854	2.918	2.791	3.015	3.444	4.092	4.958	5.967
22	12/16/18	61.902	61.893	7.551	3.026	2.780	2.955	3.345	3.954	4.780	5.745
23	12/26/18	61.808	61.898	61.766	3.293	2.779	2.905	3.253	3.821	4.609	5.531
24	1/5/19	61.674	61.835	61.850	10.866	2.783	2.868	3.173	3.697	4.444	5.326
25	1/15/19	61.505	61.734	61.817	61.811	2.789	2.855	3.112	3.585	4.289	5.128
26	1/25/19	61.303	61.598	61.747	61.803	61.555	2.945	3.087	3.493	4.146	4.942
27	2/4/19	61.069	61.429	61.642	61.761	61.786	4.473	3.167	3.439	4.024	4.769
28	2/14/19	60.806	61.229	61.506	61.687	61.783	61.358	3.736	3.469	3.934	4.614
29	2/24/19	60.515	61.000	61.339	61.582	61.742	61.725	9.982	3.745	3.905	4.487
30	3/6/19	60.196	60.742	61.143	61.446	61.668	61.740	61.252	5.097	4.017	4.405
31	3/16/19	59.851	60.457	60.918	61.280	61.563	61.704	61.697	18.634	4.530	4.409
32	3/26/19	59.481	60.145	60.666	61.087	61.429	61.632	61.732	61.168	6.698	4.603
33	4/5/19	59.088	59.809	60.387	60.865	61.266	61.529	61.701	61.704	26.615	5.329
34	4/15/19	58.672	59.449	60.083	60.618	61.075	61.396	61.632	61.762	61.029	8.133
35	4/25/19	58.234	59.065	59.755	60.345	60.858	61.236	61.530	61.739	61.689	30.399
36	5/5/19	57.776	58.659	59.403	60.047	60.615	61.049	61.399	61.672	61.773	60.866
37	5/15/19	57.299	58.232	59.029	59.725	60.347	60.836	61.241	61.573	61.758	61.707
38	5/25/19	56.802	57.785	58.633	59.380	60.055	60.597	61.056	61.444	61.696	61.823
39	6/4/19	56.288	57.318	58.215	59.013	59.740	60.334	60.845	61.288	61.599	61.818

Figure 1. This short-way Earth-to-Mars PCC summarizes asymptotic Earth departure speed v_D (in km/s) around the time of InSight's interplanetary cruise, with v_D values less than 6.0 km/s colored green. Boxes circumscribe viable Earth depart dates and the single Mars arrive date targeted for InSight's landing.

[3] The value v_D^2 is equivalent to the parameter $C3$ often used in Earth departure trajectory design [2, p. 23].

◇	A	B	C	D	E	F	G	H	I	J	K
1	**Mars Arrive**	**Earth Depart Date**									
2	**Date**	4/5/18	4/15/18	4/25/18	5/5/18	5/15/18	5/25/18	6/4/18	6/14/18	6/24/18	7/4/18
3	6/9/18	-20.635	-20.508	-20.664	-20.962	-21.306	-21.572	-21.707			
4	6/19/18	-20.579	-20.310	-20.409	-20.728	-21.174	-21.578	-21.856	-21.993		
5	6/29/18	-20.840	-20.420	-20.446	-20.766	-21.300	-21.834	-22.249	-22.515	-22.620	
6	7/9/18	-21.471	-20.902	-20.855	-21.168	-21.781	-22.429	-22.960	-23.329	-23.504	-23.558
7	7/19/18	-22.517	-21.807	-21.698	-22.008	-22.693	-23.432	-24.039	-24.458	-24.636	-24.680
8	7/29/18	-24.011	-23.165	-23.007	-23.322	-24.075	-24.863	-25.477	-25.858	-25.946	-25.892
9	8/8/18	-25.968	-24.978	-24.778	-25.100	-25.900	-26.663	-27.181	-27.403	-27.291	-27.053
10	8/18/18	-28.385	-27.219	-26.961	-27.270	-28.061	-28.686	-28.974	-28.908	-28.500	-28.015
11	8/28/18	-31.232	-29.816	-29.451	-29.689	-30.375	-30.716	-30.639	-30.184	-29.433	-28.683
12	9/7/18	-34.465	-32.665	-32.097	-32.167	-32.618	-32.532	-31.993	-31.112	-30.028	-29.039
13	9/17/18	-38.047	-35.645	-34.729	-34.503	-34.585	-33.973	-32.945	-31.664	-30.300	-29.120
14	9/27/18	-42.000	-38.659	-37.196	-36.536	-36.144	-34.979	-33.497	-31.884	-30.306	-28.983
15	10/7/18	-46.471	-41.672	-39.404	-38.168	-37.249	-35.562	-33.701	-31.836	-30.107	-28.684
16	10/17/18	-51.848	-44.766	-41.329	-39.371	-37.908	-35.773	-33.618	-31.577	-29.747	-28.258
17	10/27/18	-58.854	-48.212	-43.035	-40.159	-38.150	-35.653	-33.288	-31.140	-29.253	-27.724
18	11/6/18	-67.109	-52.624	-44.694	-40.578	-37.996	-35.218	-32.726	-30.534	-28.631	-27.090
19	11/16/18	-44.251	-59.255	-46.667	-40.695	-37.439	-34.451	-31.915	-29.748	-27.873	-26.351
20	11/26/18	17.571	-67.834	-49.771	-40.625	-36.448	-33.299	-30.810	-28.750	-26.960	-25.494
21	12/6/18	20.483	7.701	-56.178	-40.608	-34.957	-31.667	-29.340	-27.490	-25.861	-24.501
22	12/16/18	21.238	18.823	-68.084	-41.266	-32.844	-29.407	-27.394	-25.900	-24.532	-23.345
23	12/26/18	21.487	19.888	16.006	-45.074	-29.821	-26.260	-24.809	-23.878	-22.918	-21.994
24	1/5/19	21.534	20.106	18.133	-66.164	-24.942	-21.714	-21.327	-21.285	-20.940	-20.404
25	1/15/19	21.474	20.068	18.326	16.283	-12.299	-14.510	-16.492	-17.907	-18.490	-18.515
26	1/25/19	21.348	19.914	18.192	16.330	18.403	-0.512	-9.393	-13.404	-15.414	-16.251
27	2/4/19	21.178	19.696	17.940	16.035	14.562	37.724	2.089	-7.180	-11.477	-13.501
28	2/14/19	20.974	19.436	17.630	15.658	13.787	16.400	23.271	1.896	-6.303	-10.108
29	2/24/19	20.744	19.147	17.285	15.247	13.188	11.955	60.678	16.060	0.745	-5.833
30	3/6/19	20.492	18.836	16.918	14.817	12.638	10.749	13.467	38.818	10.789	-0.298
31	3/16/19	20.223	18.507	16.534	14.375	12.109	9.944	8.895	63.617	25.667	7.110
32	3/26/19	19.937	18.163	16.137	13.925	11.589	9.269	7.411	10.397	46.877	17.388
33	4/5/19	19.637	17.807	15.730	13.469	11.075	8.652	6.456	5.604	57.252	31.896
34	4/15/19	19.325	17.440	15.314	13.007	10.563	8.066	5.687	3.900	7.444	50.688
35	4/25/19	19.001	17.064	14.890	12.540	10.053	7.498	5.005	2.825	2.257	51.446
36	5/5/19	18.667	16.678	14.459	12.070	9.544	6.942	4.371	1.983	0.347	4.824
37	5/15/19	18.323	16.285	14.023	11.595	9.035	6.395	3.767	1.254	-0.833	-0.994
38	5/25/19	17.970	15.884	13.580	11.118	8.526	5.854	3.183	0.588	-1.735	-3.126
39	6/4/19	17.609	15.477	13.133	10.637	8.016	5.316	2.612	-0.039	-2.499	-4.406

Figure 2. This short-way Earth-to-Mars PCC summarizes asymptotic Earth departure declination δ_D (in decimal degrees) around the time of InSight's interplanetary cruise, with | δ_D | values less than 58.0° colored green. Boxes circumscribe viable Earth depart dates and the single Mars arrive date targeted for InSight's landing.

Coloration thresholds applied to Figure 1 and Figure 2 values are to some degree arbitrary. The v_D < 6.0 km/s criterion for green coloration in Figure 1 is adopted in lieu of published InSight-specific Atlas V 401 performance limits and serves to define the mission's approximate interplanetary cruise interval. Figure 2's | δ_D | < 58.0° criterion for green coloration is attributable to the maximum orbit inclination permissible for CCAFS launches [3, p. SR-3]. Thus, there are no viable InSight VAFB launch dates on which a CCAFS launch targeting Mars could not also be conducted within range safety limits.

Focusing on 5 May 2018 as the patched conic design's t_D, a geocentric asymptotic departure velocity $\boldsymbol{v_D}$ is computed. This vector is the axis of symmetry for a manifold of geocentric Earth departure trajectories leading to short way Mars intercepts at t_A = 26 November 2018 (reference [2, p. 114, Fig. 6.16] for an illustration of this symmetric manifold). All trajectories in the geocentric departure manifold are aligned with $\boldsymbol{v_D}$ as they enter interplanetary space on a geocentric escape hyperbolic trajectory with this common asymptote. Since TMI $\boldsymbol{\Delta v}$ is assumed to contain no planar correction, the Earth parking orbit leading to TMI must lie in a plane containing $\boldsymbol{v_D}$. With launch assumed to be instantaneous, the VAFB geocentric position vector at launch $\boldsymbol{r_{LO}}$[4] must also lie in this plane. Thus, the parking orbit plane's normal is defined by the vector product $\boldsymbol{r_{LO}} \times \boldsymbol{v_D}$. Figure 3 illustrates how VAFB launch azimuth ψ varies throughout the 5 May 2018 UTC day as $\boldsymbol{r_{LO}}$ undergoes rotation about Earth's polar axis in inertial space. Because prograde ψ in Figure 3 is further restricted to values exceeding 150° by VAFB range safety [3, p. SR-4], the May 5 launch window for this design extends from about 12:00 to 15:00 UTC[5].

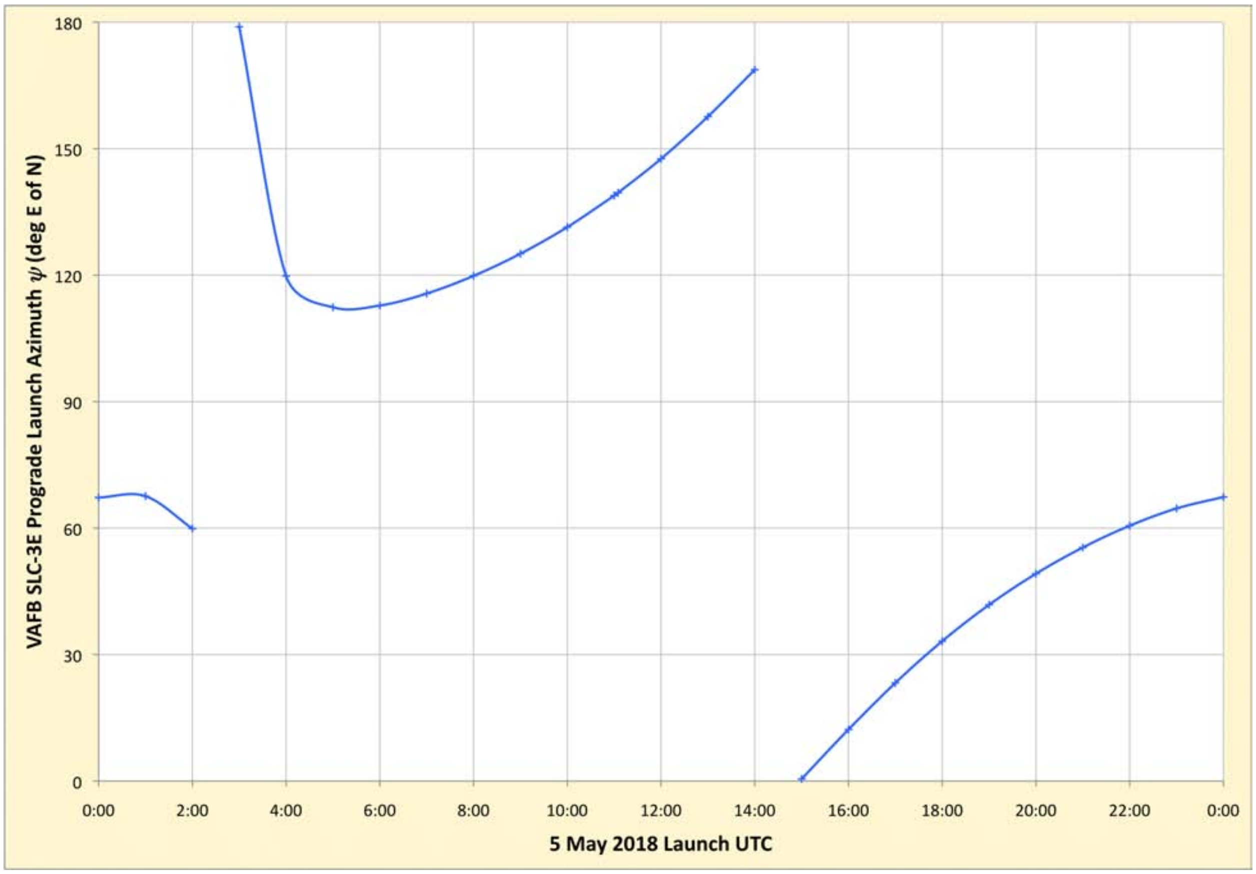

Figure 3. Launch azimuth from VAFB instantaneously achieving a parking orbit coplanar with short way departures for Mars is plotted as a function of launch UTC throughout 5 May 2018.

The launch window inferred from Figure 3 notably excludes InSight's actual launch time at 11:05 UTC. Coplanar trajectory assumptions adopted for Figure 3 launch azimuths are evidently inconsistent with at least the first half of the actual InSight launch window extending from 11:05 to 13:05 UTC on 5 May 2018. In the interest of more relevant comparison with InSight's as-flown Earth departure, the coplanar trajectory design therefore ignores VAFB launch azimuth limits and adopts an instantaneous launch time of 11:05 UTC with $\psi = 139.542°$ and $i = 57.732°$ in the resulting parking orbit. See the Appendix for details on how to compute i from ψ and ϕ.

---

[4] Geocentric position for SLC-3E used herein is traceable to https://www.google.com/maps/place/34%C2%B038'24.0%22N+120%C2%B035'24.0%22W/@34.6400044,-120.5921887,1191m/data=!3m2!1e3!4b1!4m5!3m4!1s0x0:0x0!8m2!3d34.64!4d-120.59 (accessed 13 May 2018).

[5] A brief interval with $\psi > 150°$ extending from about 3:00 to 3:20 UT is discarded as operationally impractical.

A different perspective on Figure 3 launch azimuth variations is provided by applying the parking orbit's $\boldsymbol{r_{LO}} \times \boldsymbol{v_D}$ constraint to the 11:05 UTC launch from VAFB and projecting the resulting parking orbit plane onto a celestial sphere plot (CSP). When regarding a CSP on a flat orthogonal grid, as in Figure 4, it is important to recall directions differ from those on a conventional Earth surface map because the celestial sphere is being viewed from its *inside*. Consequently, although north is upward on a CSP, east is *leftward* from this interior perspective.

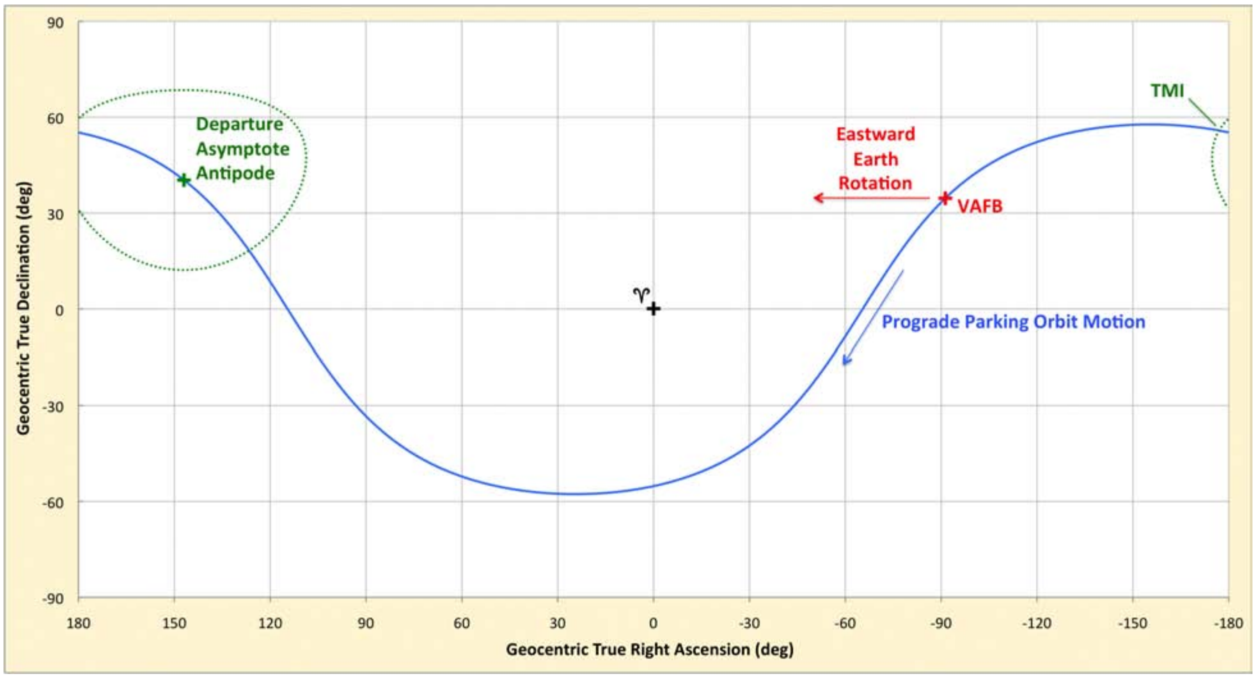

Figure 4. The dotted small circle centered on the departure asymptote antipode (green "+" marker) is the locus of possible injection points (LPIP) for TMI on 5 May 2018. It and VAFB position at 11:05 UTC launch (red "+" marker) define the parking orbit plane's great circle in inertial space (blue). Following launch and antipode passage in the parking orbit, a purely prograde TMI impulse is performed as the LPIP-enclosed region is exited. For reference, direction to the Sun's geocentric position at the Spring Equinox is indicated with a black "+" marker annotated by "♈".

The departure asymptote antipode and its circumscribing LPIP are virtually fixed in Figure 4's CSP throughout the UTC day on 5 May 2018, but VAFB shifts left (eastward) at a rate near 15°/hour as Earth's surface rotates in inertial space. Near 15:00 UTC, following 4 hours of Earth rotation from its Figure 4 location, VAFB lies very nearly 180° in right ascension from the antipode. During the 4 hours, VAFB ψ has been increasing from 139.542° at 11:05 UTC to nearly 180° (due south). The Figure 3 jump to $\psi = 0$ occurs near 15:00 UTC in order to maintain VAFB launch into a prograde parking orbit.[6]

[6] This northerly launch from VAFB would grossly violate range safety constraints with Atlas V 401 powered flight over central California.

As a final check on the coplanar design's validity, parking orbit velocity at TMI is scaled up such that its speed is consistent with the 5 May 2018 v_D in Figure 1. The resulting impulsive TMI "burnout" state vector is coasted via numeric integration [4] while modeling gravity from the Earth, Sun, and Mars as point sources. Closest approach to Mars then occurs at 02:57 UTC on 23 November 2018 (3 days early with respect to the PCC Mars arrival date in Figures 1 and 2) with Mars H = +245,810 km. These Mars periapsis deviations in time and position could readily be removed by applying differential correction iterations to this coast's initial velocity at TMI burnout.

As-Flown Trajectory Reconstruction From Launch To Heliocentric Cruise

Data critical to this reconstruction are obtained from two external sources. First, telemetry-driven digital data are gathered from launch coverage video and animation posted at https://www.youtube.com/watch?v=EF-hLs4F2uE (accessed 15 May 2018). Notable events in this video and animation are summarized in Table 1.

Table 1. Key trajectory reconstruction events from telemetry-driven InSight launch coverage video and animation are noted. The Time column reproduces H:MM:SS as displayed by YouTube.com's video player. Time since launch in H:MM:SS mission elapsed time (MET) is associated with some events.

Time	Event
0:37:38	Liftoff at 11:05:00 UTC
0:42:09	Shortly after Centaur-2 ignition, ψ = 153.5°
0:51:04	Centaur-2 MECO-1 at 0:13:21 MET with HAxHP = 100x100 nm and i = 64°
1:57:07	Centaur-2 TMI ignition at 1:19:00 MET (12:24:00 UTC) with i = 64°
2:02:08	Just before Earth escape speed during TMI (and loss of digital displays), i = 63.636°
2:02:30	Centaur-2 MECO-2 at 1:24:23 MET

A snapshot of launch coverage animation at 1:19:00 MET appears in Figure 5 as TMI begins.

Figure 5. The "4739.67" readout at lower left from this InSight launch coverage animation snapshot is MET in seconds, equivalent to 1:19:00 MET in Table 1 when TMI is initiated. Note how the Centaur-2 thrust vector appears biased upward with respect to the horizon and inward with respect to the animation display.

A Space Shuttle launch simulator[7] is configured to duplicate Table 1's MECO-1 conditions starting from liftoff at SLC-3E. Because these conditions are achieved with only Solid Rocket Motor and Main Propulsion System thrust (no Orbit Maneuvering System propulsion is required), Shuttle ascent guidance accomplishes the task at 0:08:33.5 MET, 4.8 minutes earlier than the as-flown MECO-1. Nevertheless, the Figure 6 ground track and TMI location resulting from this reconstructed launch are in reasonable agreement with the world map inset appearing in Figure 5.

[7] Reference the MacMECO application at http://home.earthlink.net/~adamod/MacMECO/MacMECO.html (accessed 16 May 2018). Note this simulator will only run on obsolete PowerPC-based Mac platforms.

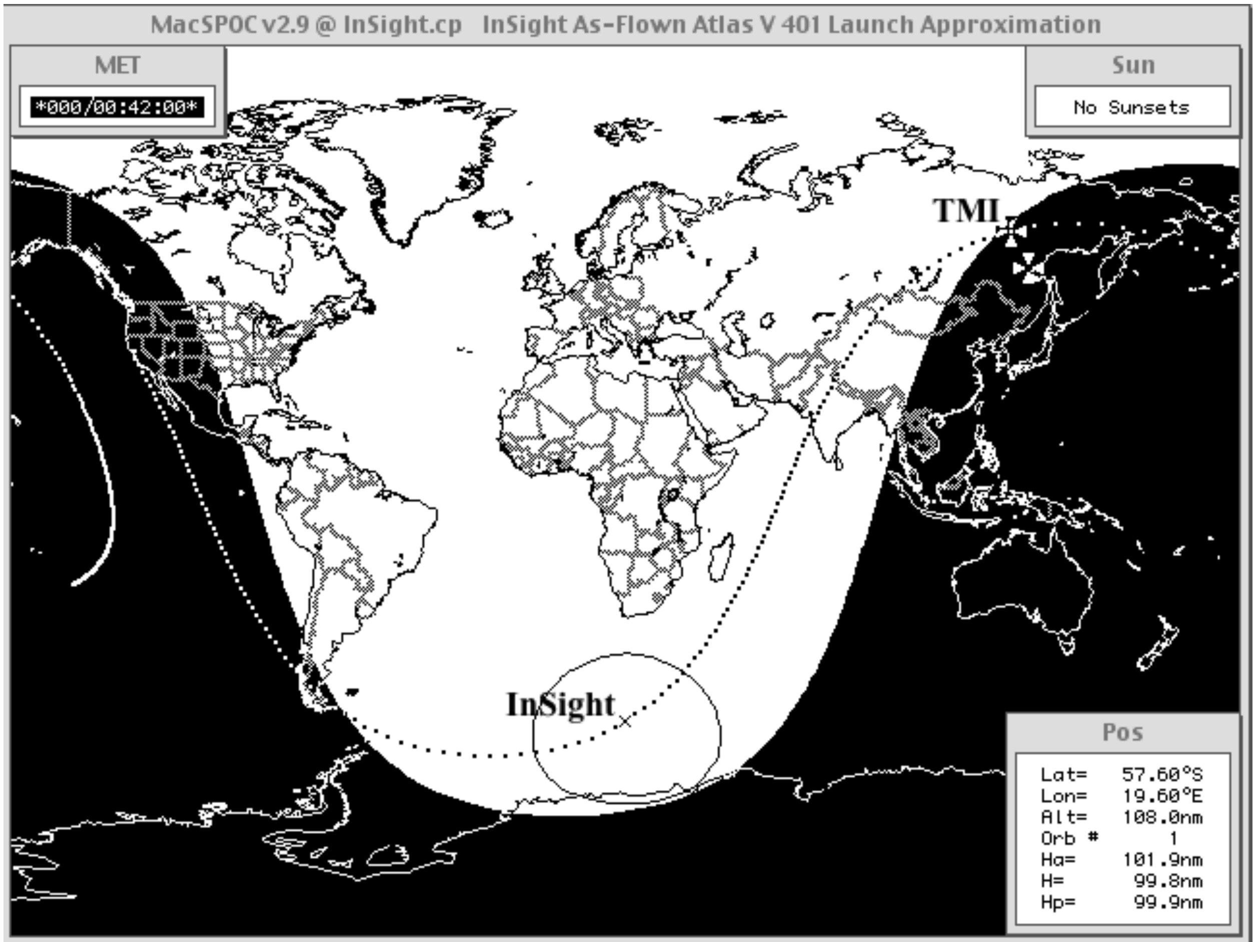

Figure 6. The reconstructed *i* = 64° InSight ground track from launch through TMI is plotted as a series of 2x2-pixel squares at 30-second intervals (these squares merge as the post-TMI trajectory recedes into deep space over the East Pacific Ocean at left). Per the "MET" window, InSight's nadir location 42 minutes after launch is the annotated "X" between South Africa and Antarctica (the circumscribing locus is a concurrent mapping of Earth horizon points consistent with InSight's position in the "Pos" window). Earth's nightside at this MET coincides with the map's reverse-field hemisphere. The iron cross icon annotated "TMI" is InSight's nadir location at 1:19:00 MET when the TMI burn begins (modeled in the plot as a purely prograde impulse at this MET). Another iron cross immediately to TMI's southeast is the purely prograde TMI impulse location associated with the coplanar trajectory design in the previous section (whose parking orbit *i* = 57.732°).

The second source of InSight trajectory reconstruction data is an as-flown geocentric state vector on 5 May 2018 at 12:38:50.815 UTC (1:33:51 MET) downloaded from JPL's *Horizons* ephemeris server.[8] Starting with the simulated MECO-1 parking orbit insertion state vector, a series of two-stage numeric integration coasts [4] is initiated simulating accelerations from Earth

[8] *Horizons* documentation and user interface information are available at https://ssd.jpl.nasa.gov/?horizons (accessed 18 May 2018). Data associated with InSight from *Horizons* as referenced herein were posted 14 May 2018 and comprise a "fit to tracking data through 2018-May-09 21:01 UTC, predicts thereafter."

gravity modeled by the Goddard Earth Model 10 (GEM-10) truncated to seventh degree and order, together with Moon and Sun gravity modeled as point sources. The first stage of each coast terminates at a specified impulsive TMI UTC, where velocity is instantaneously modified according to a perturbed Lambert solution for the coast's second stage. As TMI UTC is varied from one coast to another, each Lambert solution ensures that coast's second stage intercepts the fixed *Horizons* position at 12:38:50.815 UTC.

The two-stage coast whose TMI UTC results in a minimal velocity residual magnitude Δv_R with respect to *Horizons* as-flown InSight velocity at 12:38:50.815 UTC is adopted as TMI's as-flown trajectory reconstruction. Per this criterion, Table 2's TMI UTC iterations indicate the reconstructed TMI impulse is at 12:27:00 UTC.

Table 2. As impulsive TMI's UTC is varied in the reconstructed parking orbit, a best velocity match with *Horizons*' as-flown InSight state vector on 5 May 2018 at 12:38:50.815 UTC is sought. This match is quantified by Δv_R, the vector difference magnitude between the *Horizons* velocity and that from a numeric integration coast starting at the reconstructed TMI impulse intercepting as-flown *Horizons* position at 12:38:50.815 UTC. Impulsive TMI at 12:27:00 UTC (colored red) is adopted for the as-flown InSight trajectory reconstruction.

5 May 2018 Impulsive TMI UTC	Δv_R (km/s)
12:24:00	0.869692
12:25:00	0.617310
12:26:00	0.335423
12:26:45	0.115059
12:26:50	0.096031
12:26:55	0.082538
12:27:00	**0.077934**
12:27:05	0.084096
12:28:00	0.393782

Per Table 1, the first TMI UTC in Table 2 is at the start of an as-flown Centaur-2 powered flight arc spanning 323 s. The midpoint of this arc is at 12:26:41.5 UTC, less than 20 s before the best impulsive approximation in Table 2. This degree of correlation between a powered flight arc and an impulse at that arc's midpoint is typical and might have been even greater had a better approximation of the as-flown InSight parking orbit been available. Although InSight received a NORAD catalog ID of 43457, no orbit elements associated with this launch had been published to Space-Track.org as of 20 May 2018.

The previous coplanar trajectory design's impulsive TMI is compared with as-flown impulsive TMI reconstruction in Table 3. This comparison is facilitated by expressing TMI change-in-velocity using three mutually orthogonal Cartesian components aligned with the geocentric UVW coordinate system defined by the pertinent parking orbit immediately before TMI: Δv_U (positive radial outward from the geocenter toward TMI position), Δv_V (positive prograde in the local horizontal plane), and Δv_W (positive along the more northerly direction orthogonal to the parking orbit plane).

Table 3. Impulsive InSight TMI parameters from the previously documented coplanar design and the present as-flown reconstruction are juxtaposed for comparison.

Parameter	Coplanar TMI Design	As-Flown Reconstructed TMI
Parking Orbit i	57.732°	63.967°
TMI 5 May 2018 UTC	12:18:34.606	12:27:00
TMI Declination	+55.833°	+63.748°
TMI Longitude	135.292° E	157.291° E
Δv_U	0	+1.344502 km/s
Δv_V	+3.591899 km/s	+3.296456 km/s
Δv_W	0	+2.315170 km/s

The UVW components of as-flown reconstructed TMI impulsive change-in-velocity in Table 3 are equivalent to thrusting along a vector whose projection into the local horizontal plane is 35.081° north of the prograde +$\boldsymbol{V}$ direction. Furthermore, the thrust vector is elevated 18.457° above the local horizontal. This significant departure from purely prograde TMI thrust is confirmation of expected robust launch vehicle performance margins. By watching InSight's launch coverage animation during TMI, this thrust vector orientation is qualitatively confirmed. Over but a few seconds of viewing, the +$\boldsymbol{V}$ direction is seen to be rightward, and the viewer's gaze is therefore in the +$\boldsymbol{W}$ direction. Thus, all UVW components of thrust in Figure 5 appear positive from the Centaur-2 rendering, just as independently reconstructed in Table 3's third column.

Another comparison with the coplanar TMI design is enabled by InSight's state vector at 12:38:50.815 UTC as posted to *Horizons*. When this state is coasted [4], again modeling only point source Earth/Sun/Mars gravity, Mars closest approach occurs at 8:27 UTC on 26 November 2018 (3.2 days later than the coplanar TMI coast) with Mars H = +147,066 km. This miss is to some degree intentional, ensuring Centaur-2 and secondary payloads [1, pp. 56-59] accompanying InSight through TMI do not enter the atmosphere of Mars and pose a contamination threat. Small course corrections by InSight during its interplanetary cruise will establish and maintain atmospheric entry conditions designed to achieve an intact Mars landing [1, p. 22].

When the *Horizons* InSight state vector at 12:38:50.815 UTC is coasted back to Table 1's TMI burnout at 12:29:23 UTC and coasted forward to 5 May 2018 at 18:00 UTC, the Figure 7 trajectory plot results. These numeric integrations [4] model Earth, Sun, and Mars gravity as point sources.

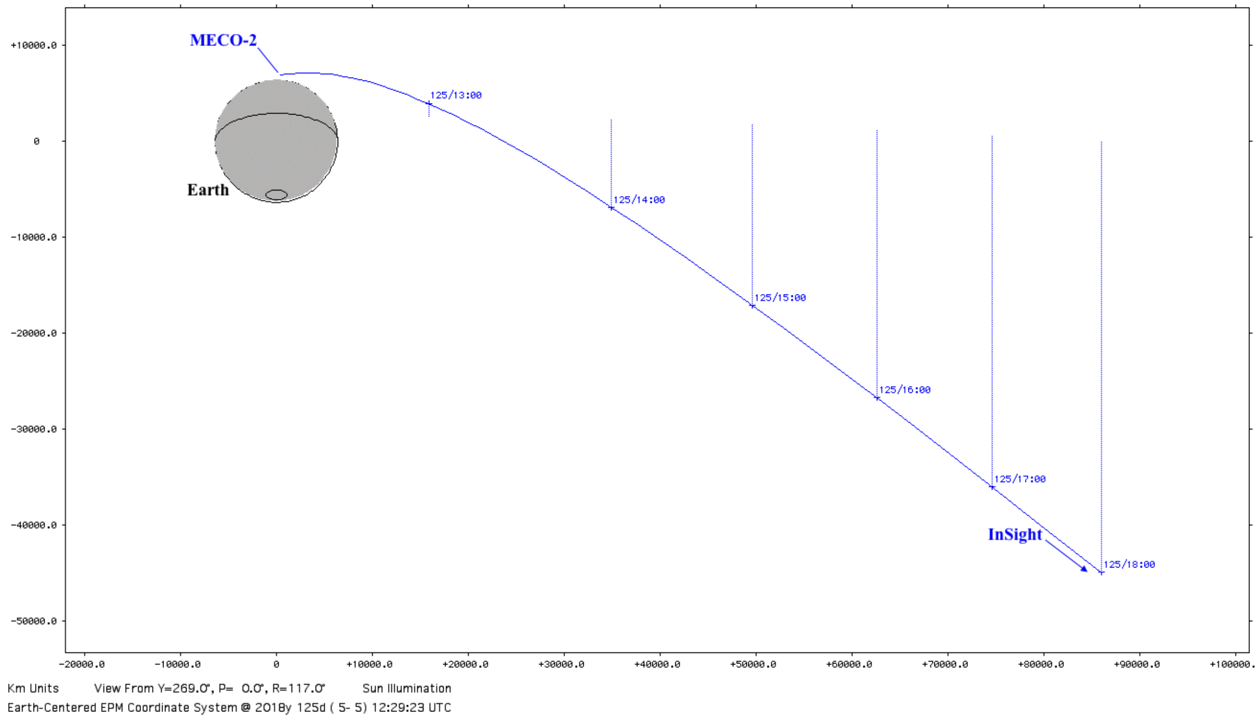

Figure 7. Post-MECO-2 InSight inertial geocentric motion is plotted with "+" time tick markers at hourly intervals annotated in UTC DOY/HH:MM format for 5 May 2018. Dotted lines from each marker are projections onto Earth's equatorial plane. This plot is viewed from nearly normal to the plane of InSight geocentric motion as it begins to achieve asymptotic Earth departure conditions near δ_D = -40.625° for Mars intercept per Figure 2. Earth's nightside is shaded, and its heliocentric motion is to the right. If the Sun were plotted, it would peek out from behind Earth's limb at about 5 o'clock.

Figure 8 illustrates InSight's geocentric motion on a larger scale than Figure 7 and plots the coplanar design[9] alongside the as-flown trajectory posted to *Horizons*. Efficient departures for Mars occur over locations near Earth's sunrise terminator (as illustrated in Figure 7), and this is also the direction to the Moon in its last quarter phase. With the Moon reaching last quarter at 8.1 May 2018 UTC[10], InSight departure in the Moon's general direction is confirmed in Figure 8.

[9] This plot arises from the numeric integration coast reaching Mars periapsis at 02:57 UTC on 23 November 2018 with H = +245,810 km, as previously reported herein.
[10] Reference the calculator at http://aa.usno.navy.mil/data/docs/MoonPhase.php (accessed 22 May 2018).

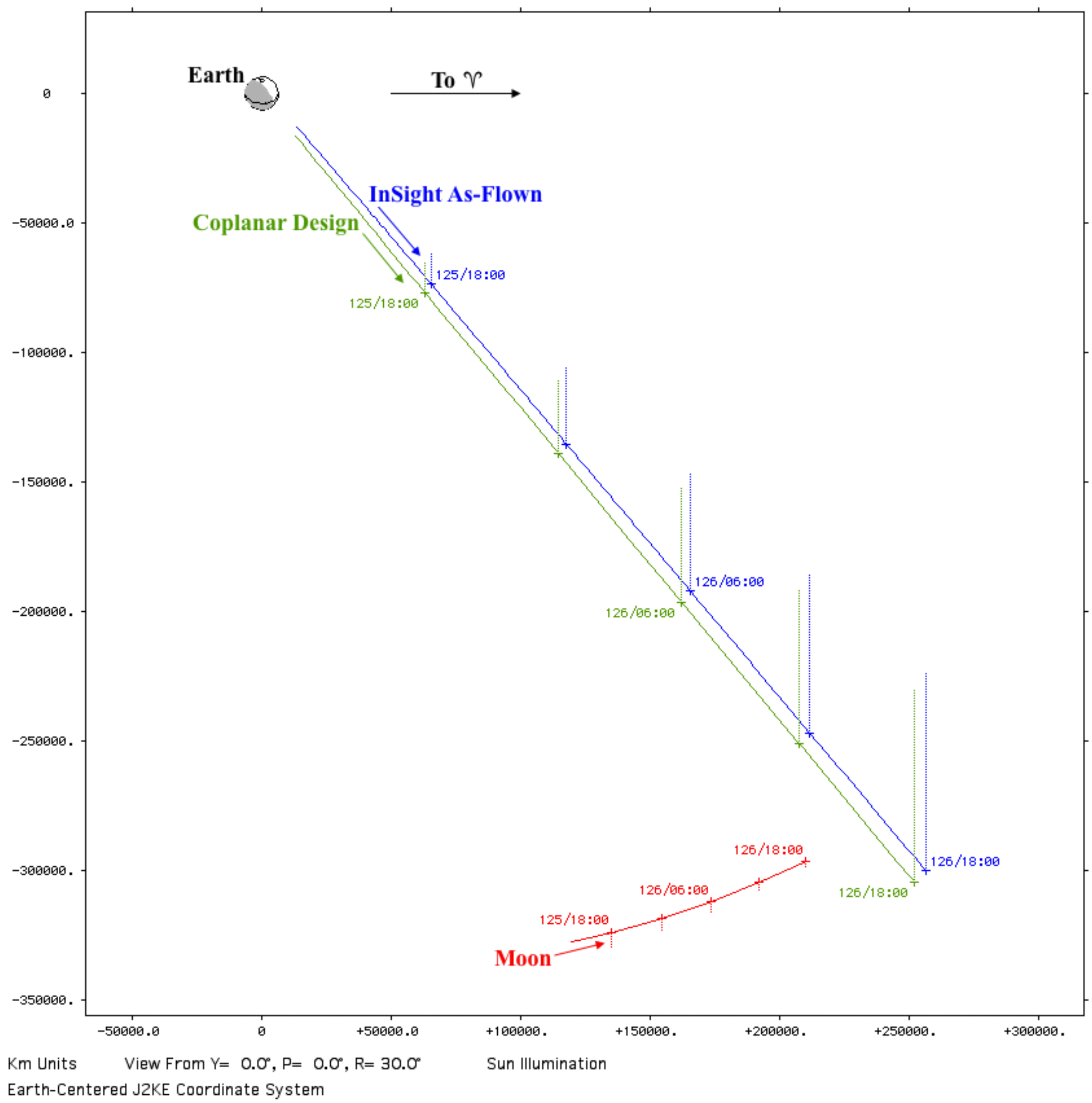

Figure 8. Using data posted to *Horizons*, InSight's as-flown geocentric inertial motion from 5 May 2018 at 12:38:50.815 UTC to 6 May 2018 at 18:00 UTC (blue) is co-plotted with that for the coplanar trajectory design (green). The Moon's motion during this time interval is also plotted (red). Time ticks at 6-hour intervals are accompanied by dotted line projections onto the ecliptic plane. Direction to the Sun's geocentric position at the Spring Equinox is annotated "To ♈". Earth's shaded region is its nightside.

InSight's heliocentric trajectory from Earth to Mars is plotted in Figure 9. At this interplanetary scale, the coplanar trajectory design is undistinguishable from corresponding data posted to *Horizons*.

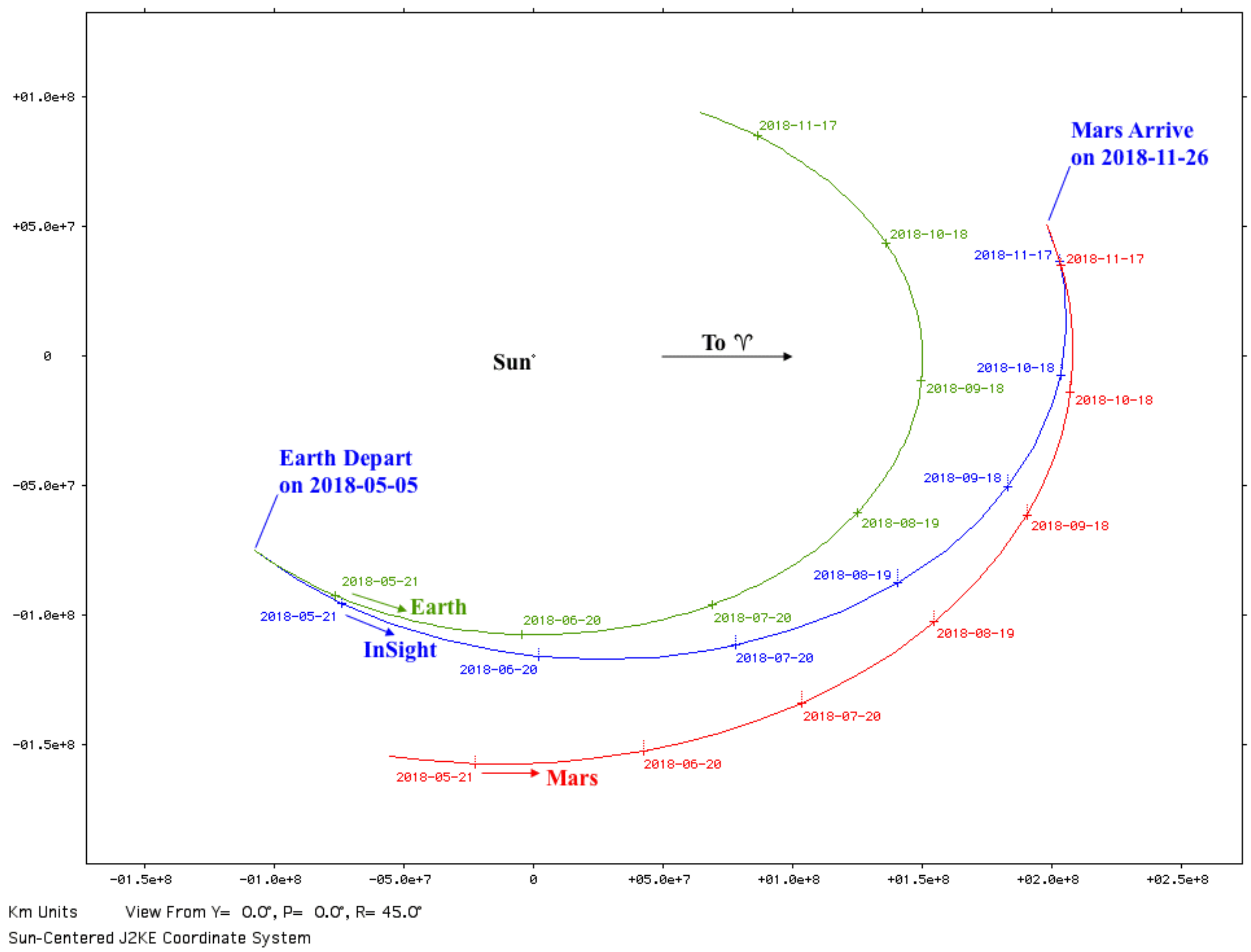

Figure 9. Inertial heliocentric motion of Earth (green), Mars (red), and InSight (blue) are plotted during the mission's planned 7-month interplanetary cruise. Time ticks at 30-day intervals are accompanied by dotted line projections onto the ecliptic plane. Note how InSight position below the ecliptic plane following Earth departure contributes to δ_D = -40.625°.

Summary

A trajectory design enabling Earth departure for Mars has been documented under the assumption its parking orbit is coplanar with the ensuing escape hyperbola. This design has demonstrated VAFB can launch missions to Mars along with the utility of patched conic theory in approximating InSight's as-flown departure. Due to relatively large launch vehicle performance margins, degrees of freedom deviating from the coplanar design permit significant excursions from the parking orbit plane during InSight's as-flown TMI, thereby affecting launch azimuth and the 5 May 2018 launch window open time. Despite these excursions, the coplanar design succeeds in replicating salient features in the as-flown InSight trajectory.

Particularly in its pre-TMI phases, reconstructing the as-flown InSight trajectory is challenged by a dearth of publicly available data. Key to filling this void is launch video and animation through TMI as posted to YouTube. Accurate post-TMI as-flown trajectory data are available from JPL's *Horizons* ephemeris server, as is the case with most interplanetary missions.

References

[1] NASA, "Mars InSight Launch Press Kit", 2008.[11]
[2] Brown, C. D., *Spacecraft Mission Design*, AIAA Education Series, 1992.
[3] FAA Associate Administrator for Commercial Space Transportation, "Special Report: An Overview of the U.S. Commercial Space Launch Infrastructure", Federal Aviation Administration, 1998.[12]
[4] Adamo, D. R., "A Precision Orbit Predictor Optimized for Complex Trajectory Operations", AAS 03-665, *Volume 116 of the Advances in the Astronautical Sciences*, Univelt, San Diego, pp. 2567-2586, 2003.

[11] This publication is available for download at https://www.jpl.nasa.gov/news/press_kits/insight/download/mars_insight_launch_presskit.pdf (accessed 8 May 2018).
[12] This report is available for download at https://www.faa.gov/about/office_org/headquarters_offices/ast/media/sr_98_3q.pdf (accessed 10 May 2018).

Appendix: Orbit Inclination From Launch Azimuth & Latitude

Given a launch site at planetocentric latitude ϕ and a launch azimuth from true north (measured positive toward true east) ψ, find the resulting true equatorial orbit inclination i. Relationships between these variables naturally arise from the Node-to-Topocentric transformation $\mathrm{M}_{\mathrm{NOD}}^{\mathrm{TOP}}$ as developed herein. The Cartesian planetocentric Node coordinate system is defined with the following mutually orthogonal unit vectors.

$\boldsymbol{I} \equiv$ directed at the orbit's ascending node on the planet's true equator
$\boldsymbol{J} \equiv$ directed 90° east of $\boldsymbol{I}$ on the planet's true equator
$\boldsymbol{K} \equiv$ directed at the planet's "north" rotational pole

Another set of mutually orthogonal unit vectors defines the Cartesian planetocentric Topocentric coordinate system.

$\boldsymbol{I'} \equiv$ directed at the launch site
$\boldsymbol{J'} \equiv$ directed at true north in the launch site's local horizontal plane ($\psi = 0$)
$\boldsymbol{K'} \equiv$ directed at true west in the launch site's local horizontal plane ($\psi = +270° = -90°$)

The Node-to-Topocentric transformation $\mathrm{M}_{\mathrm{NOD}}^{\mathrm{TOP}}$ results from three Euler rotations as follows.

1) A roll through $+i$
2) A yaw through $+u$, the orbit's argument of latitude at the launch site
3) A roll through $+\psi$

This Euler sequence is then expressed in matrix form and multiplied to produce $\mathrm{M}_{\mathrm{NOD}}^{\mathrm{TOP}}$.

$$\mathrm{M}_{\mathrm{NOD}}^{\mathrm{TOP}} = \begin{bmatrix} 1 & 0 & 0 \\ 0 & \cos\psi & \sin\psi \\ 0 & -\sin\psi & \cos\psi \end{bmatrix} \begin{bmatrix} \cos u & \sin u & 0 \\ -\sin u & \cos u & 0 \\ 0 & 0 & 1 \end{bmatrix} \begin{bmatrix} 1 & 0 & 0 \\ 0 & \cos i & \sin i \\ 0 & -\sin i & \cos i \end{bmatrix}$$

$$\mathrm{M}_{\mathrm{NOD}}^{\mathrm{TOP}} = \begin{bmatrix} 1 & 0 & 0 \\ 0 & \cos\psi & \sin\psi \\ 0 & -\sin\psi & \cos\psi \end{bmatrix} \begin{bmatrix} \cos u & \cos i \sin u & \sin i \sin u \\ -\sin u & \cos i \cos u & \sin i \cos u \\ 0 & -\sin i & \cos i \end{bmatrix}$$

$$\mathrm{M}_{\mathrm{NOD}}^{\mathrm{TOP}} = \begin{bmatrix} \cos u & \cos i \sin u & \sin i \sin u \\ -\sin u \cos\psi & \cos i \cos u \cos\psi - \sin i \sin\psi & \sin i \cos u \cos\psi + \cos i \sin\psi \\ \sin u \sin\psi & -\cos i \cos u \sin\psi - \sin i \cos\psi & -\sin i \cos u \sin\psi + \cos i \cos\psi \end{bmatrix}$$

The first relationship of interest is the $\boldsymbol{K}$ component of $\boldsymbol{I'}$ derived per Equation 1 from the launch site's known planetocentric latitude ϕ.

$$\boldsymbol{K} \bullet \left[\mathrm{M}_{\mathrm{NOD}}^{\mathrm{TOP}}\right]^{\mathrm{T}} \begin{bmatrix} 1 \\ 0 \\ 0 \end{bmatrix} = \sin i \sin u = \sin\phi \qquad (1)$$

Appendix: Orbit Inclination From Launch Azimuth & Latitude

The second relationship of interest arises in Equation 2 from the definition of $\boldsymbol{J'}$, as its planetocentric latitude is $\phi + 90°$ and $\sin(\phi + 90°) = \cos\phi$.

$$\boldsymbol{K} \bullet \left[\mathrm{M}_{\mathrm{NOD}}^{\mathrm{TOP}}\right]^{\mathrm{T}} \begin{bmatrix} 0 \\ 1 \\ 0 \end{bmatrix} = \sin i \cos u \cos \psi + \cos i \sin \psi = \cos \phi \qquad (2)$$

The third relationship of interest arises from the definition of $\boldsymbol{K'}$, as it is parallel to the $\boldsymbol{I}/\boldsymbol{J}$ plane and therefore has zero $\boldsymbol{K}$ component per Equation 3.

$$\boldsymbol{K} \bullet \left[\mathrm{M}_{\mathrm{NOD}}^{\mathrm{TOP}}\right]^{\mathrm{T}} \begin{bmatrix} 0 \\ 0 \\ 1 \end{bmatrix} = \cos i \cos \psi - \sin i \cos u \sin \psi = 0 \qquad (3)$$

Solving Equation 1 for $\sin i$ and substituting into Equations 2 and 3 produces a system of two equations with two unknowns.

$$\cos i \sin \psi + \sin \phi \cot u \cos \psi = \cos \phi \qquad (4)$$
$$\cos i \cos \psi - \sin \phi \cot u \sin \psi = 0 \qquad (5)$$

Finally, solve Equation 4 for $\sin \phi \cot u$, substitute into Equation 5, and obtain the desired expression for $\cos i$.

$$\cos i \cos \psi + (\cos i \sin \psi - \cos \phi) \tan \psi = 0 \qquad (6)$$
$$\cos i = \cos \phi \sin \psi \qquad (7)$$

Equation 7 is a manifestation of Napier's 8th Rule[1] applied to the right spherical triangle whose vertices are pointed to by $\boldsymbol{I}$, $\boldsymbol{I'}$, and the equatorial planetocentric unit vector lying on the same meridian as $\boldsymbol{I'}$. Vallado[2] also obtains the Equation 7 result.

[1] Reference https://en.wikipedia.org/wiki/Spherical_trigonometry#Napier%27s_rules_for_right_spherical_triangles (accessed 13 May 2018).
[2] Reference *Fundamentals of Astrodynamics and Applications*, p. 294, Eq. 5-11, 1997.